Progress In Electromagnetics Research C, Vol. 72, 167–175, 2017

Design and Evaluation of a Dual-Load Waveguide Calorimeter

Wei He[1, 2, 3, *], Weiwei Zhang[2, 3], Chunyue Cheng[2, 3], and Hongcheng Yin[4]

Abstract—A broadband rectangular waveguide calorimeter for power sensor calibration in the millimeter-wave region is presented in this study. The calorimeter has a dual-load structure, an operational frequency range of 26.5 GHz to 40 GHz, and high substitution efficiency and sensitivity. Its effective efficiency uncertainty is $0.74\% \sim 1.1\%$.

1. INTRODUCTION

Calorimeters have been used as the primary power standard in many countries because of their high accuracy [1]. The Beijing Institute of Radio Metrology and Measurement (BIRMM) built a series of calorimeters as a microwave power standard in the 1970s. However, with reduced measurement errors of power sensors, the uncertainty of these old calorimeters could no longer satisfy the calibration requirements. In 2006, calorimeters started to be rebuilt with coaxial connectors of 100 kHz to 18 GHz and waveguide connectors of 18 to 50 GHz, and the method of effective efficiency evaluation was improved. This report presents the thermal model, structure, measurement process, evaluation, and verification results of the effective efficiency and uncertainty of a 26.5 GHz to 40 GHz waveguide calorimeter. The uncertainty is reduced by a factor of 2 relative to earlier calorimeters.

2. CALORIMETER STRUCTURE

2.1. Basic Structure of the Dual-Load Waveguide Calorimeter

The basic structure of the calorimeter features two loads (A and B) with the same thermal characteristics inside a constant-temperature container. Load A absorbs the microwave (rf) power and direct current (dc) power. Load B serves as a temperature reference, without any power input. When the rf power is absorbed by load A, the temperature increases, resulting in a temperature difference, which is measured by a thermopile installed between loads A and B. If the load has the same thermal effect for the rf and dc power input, the dc/rf power substitution method can be used to measure the rf power [2].

The dual-load waveguide calorimeter is based on a constant-temperature structure, which has high temperature stability. The dual-load structure and thermopile can smooth the temperature drift caused by temperature changes on the external of the calorimeter and thus achieve high-accuracy results. Fig. 1 shows the calorimeter structure and thermal model.

Assume that C_1 and C_2 are the thermal capacities of loads A and B, respectively; θ_1 and θ_2 are the respective load temperatures; G_1 and G_2 are the respective thermal conductivities between the load and the thermal isolation bracket. G_m is the thermal conductivity between loads A and B [3].

Received 31 December 2016, Accepted 17 March 2017, Scheduled 28 March 2017

* Corresponding author: Wei He (hewei_birmm@sina.com).

[1] The Graduate School of The Second Academy of China Aerospace, Beijing 100854, China. [2] Nation Key Laboratory of Metrology and Calibration Technology, Beijing 100854, China. [3] Beijing Institute of Radio Metrology and Measurement, Beijing 100854, China. [4] Beijing Institute of Environmental Characteristics, Beijing 100854, China.

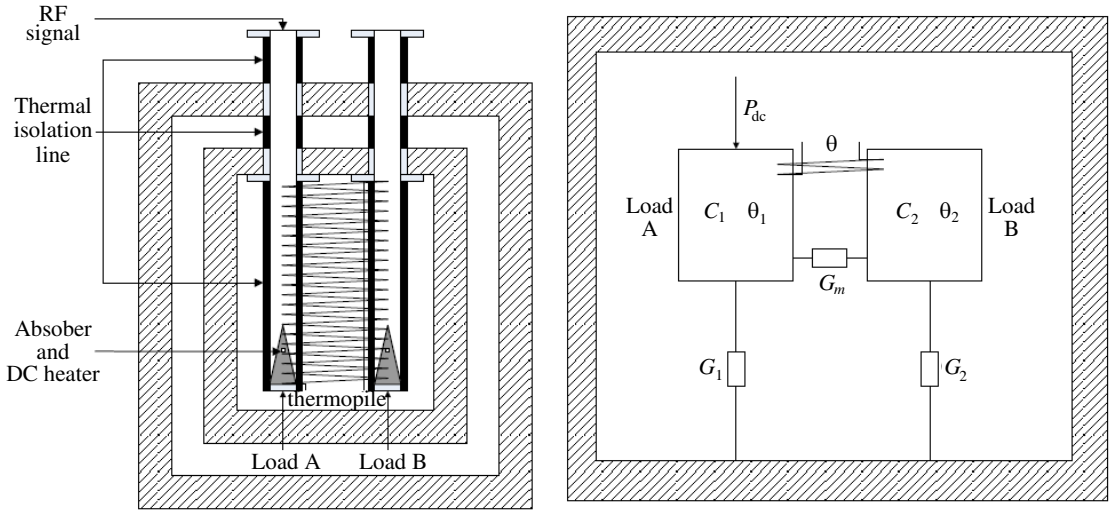

Figure 1. Structure and thermal model of the dual-load waveguide calorimeter.

With the dc power input, the temperature difference between A and B is:

$$\theta = \theta_1 - \theta_2 = \frac{P_{\rm dc}}{C_1}\tau\left(1 - e^{-\frac{t}{\tau}}\right) \tag{1}$$

The thermal constant time is:

$$\tau = \frac{C_1}{2G_m} \tag{2}$$

With the rf power input, the rf power absorbed by the calorimeter $P_{\rm rf}$ is:

$$P_{\rm rf} = P_{\rm dc}K_g\frac{\eta_d + k(1-\eta_d)}{\eta_{Ls} + k(1-\eta_{Ls})} \tag{3}$$

$P_{\rm dc}$ is the dc power absorbed by the calorimeter, and η_d is the dc power absorption efficiency of the calorimeter, which is nearly equal to 1 if dc heater is inside absorber, and its volume is small. $\eta_{Ls} = P_{{\rm rf},l}/P_{{\rm rf},c}$ is the rf power absorption efficiency of the calorimeter, $P_{{\rm rf},l}$ the rf power absorbed by load, and $P_{{\rm rf},c}$ the rf power absorbed by calorimeter. $K_g = e_{\rm dc}/e_{\rm rf}$ is the proportionality coefficient of thermopile output for the rf and dc power inputs, $e_{\rm dc}$ the thermopile output with the dc power input, and $e_{\rm rf}$ the thermopile output with the rf power input. k is proportionality coefficient of thermopile output for power loss by transmission line and power absorbed by load. η_d, η_{Ls}, and k are the characteristic parameters of the calorimeter, which can be confirmed by experiments [4].

2.2. Design of the Calorimeter Constant-Temperature Structure

The calorimeter design is based on the principle of equivalent substitution measurement through temperature differences. Thus, there should be a space in which the temperature is stable in order to reduce the influence of changes in the environmental temperature. The constant-temperature structure of the calorimeter consists of a copper outer bucket 308 mm in diameter and 30 mm in thickness, and an inner bucket 210 mm in diameter and 30 mm in thickness. The inner bucket is supported by polysulfone plastic on the bottom of the outer bucket. The structure weighs more than 200 kg and is covered with foam plastic, so it has a large thermal capacity and stable internal temperature achieved by using a temperature control system. Fig. 2 shows the constant-temperature structure of the 26.5 GHz $\sim$ 40 GHz calorimeter.

Figure 3 shows the measurement results from ten temperature sensors when temperature is stable. The sensors are located on one side of the load waveguide surface with 7 mm distance between two sensors.

As shown in Fig. 3, 7 hours after temperature had been stabilized, the standard deviation of the temperature was 0.0004 K.

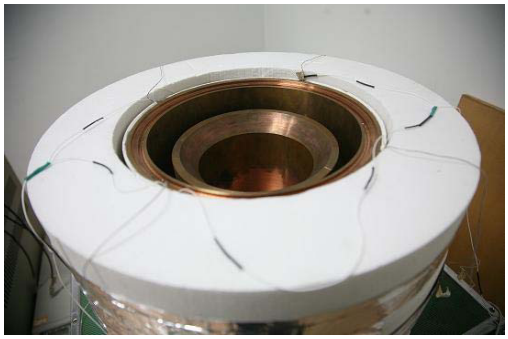

Figure 2. Constant-temperature structure of the calorimeter.

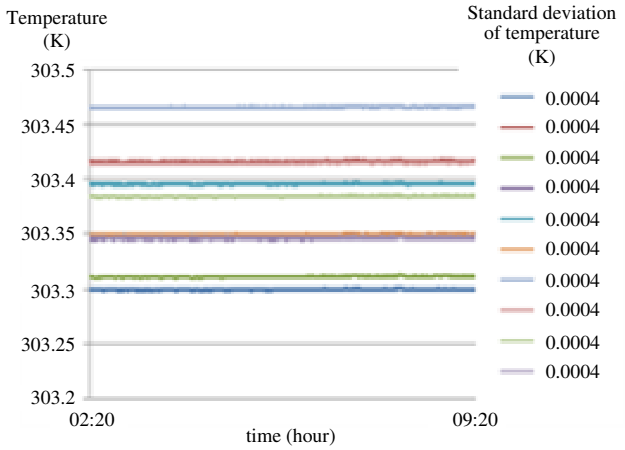

Figure 3. Temperature measurement results.

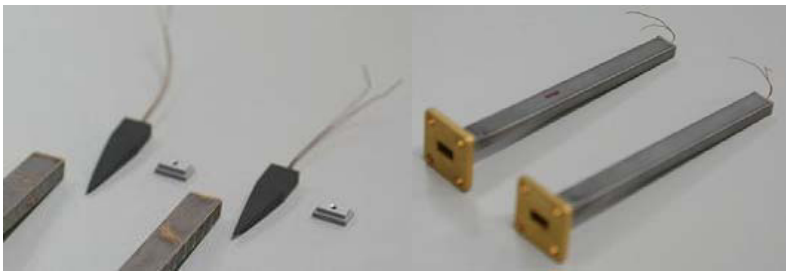

Figure 4. Structure of the load.

2.3. Design of the Load

The load of calorimeter should have a good thermal isolation effect to reduce the thermal influence of the constant-temperature structure and line, a good matching performance to absorb most of the rf power, and a high dc power heating efficiency to absorb most of the dc power.

To achieve those characteristics, the load structure of the 26.5 GHz ~ 40 GHz waveguide calorimeter includes a tapered absorber with a 0.04 mm^3-volume dc heater inside and a thin-wall (0.3 mm-thick) stainless steel waveguide, as shown in Fig. 4. Table 1 presents the simulation results for the sum of the temperature differences with ten points on load waveguide surface for the 1 mW dc and rf power absorbed by load; the sums are the same with less than 0.2% error. Fig. 5 shows the measurement results for the temperature distribution and the voltage standing wave ratio (VSWR) of the load. The sum of the temperature differences for the 5 mW dc and the rf power absorbed by load measured by 10 temperature sensors located on one side of load waveguide surface are almost the same with less than 0.3% error and are not affected by the frequency; the VSWR of the load is less than 1.1 from 26.5 GHz to 40 GHz, and the rf power absorption efficiency is more than 0.998.

The simulation and measurement results indicate that for this calorimetric load, a 0.04 mm^3-volume dc heater is very small, and its position is close to the top end of the absorber; thus, the dc heating efficiency is nearly equal to 1. The 0.3 mm-thick stainless steel waveguide of the load, which is made

Table 1. Simulation results for the sum of the heating temperature differences.

Frequency (GHz)	0	26.5	33	40
Sum of temperature differences (K)	0.3250	0.3247	0.3250	0.3252

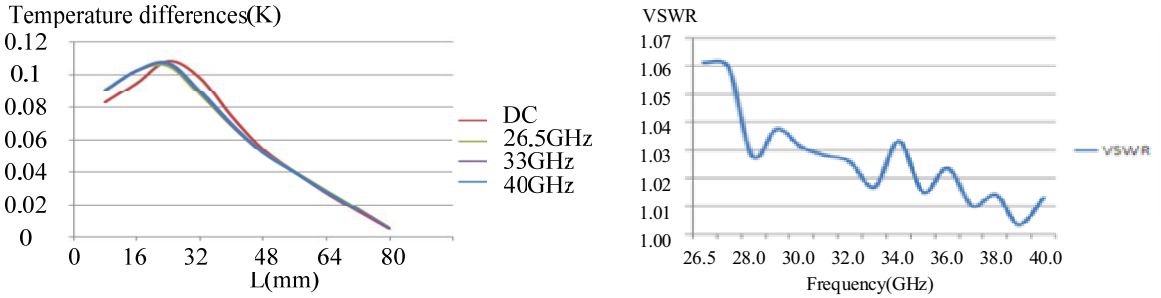

Figure 5. Measurement results for the temperature distribution and voltage standing wave ratio of the load.

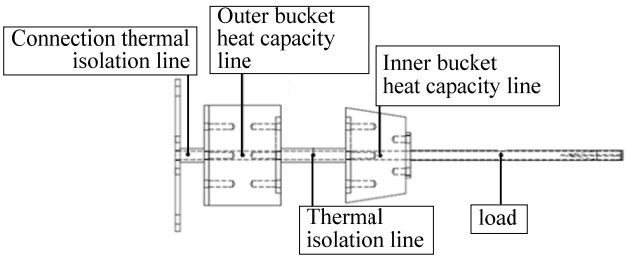

Figure 6. Thermal isolation line.

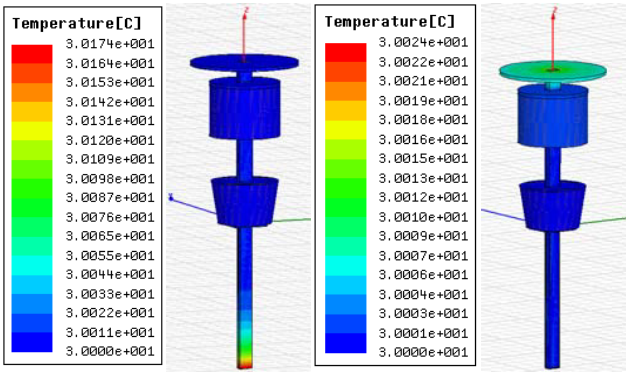

Figure 7. Simulation results for the thermal characteristics of the transmission line.

by low-speed wire-cut electrical discharge machine, has a very good thermal isolation effect; thus, the structure can reduce the temperature distribution measurement error caused by the flange.

2.4. Design of the Thermal Isolation Line

The thermal isolation line of the calorimeter consists of a connection thermal isolation line, outer and inner bucket heat capacity lines, a thermal isolation line between the outer and a inner bucket heat capacity line, as shown in Fig. 6.

Connection thermal isolation line, thermal isolation line between the outer and inner bucket heat capacity lines has a stainless steel waveguide of 0.3 mm thickness made by low-speed wire-cut electrical discharge machine to increase the heat resistance and reduce the thermal transfer from environment and constant-temperature structure. Fig. 7 shows the simulation results for the thermal characteristics of the thermal isolation line.

As shown in Fig. 7(a), the heat source is placed at the end of the load, and the power is 1 mW. The temperature change caused by thermal transfer disappears in the connector between the load and heat capacity lines, which means that the temperature increase caused by the dc and rf power is just distributed on the waveguide of the load. In Fig. 7(b), the heat source is at start of the transmission line, and the power is 1 mW. The temperature change caused by thermal transfer hardly affects the temperature distribution of the load, which indicates that this kind of thermal isolation line is suitable for our calorimeter.

2.5. Design of the Thermopile

We use a thermopile to achieve the total temperature distribution measurement on the surface of the calorimeter load. First, a copper line is adhered onto an FR4 circuit board. Then, a nickel line is

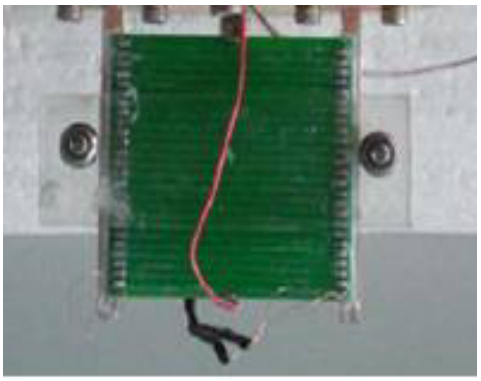

Figure 8. Structure of the thermopile.

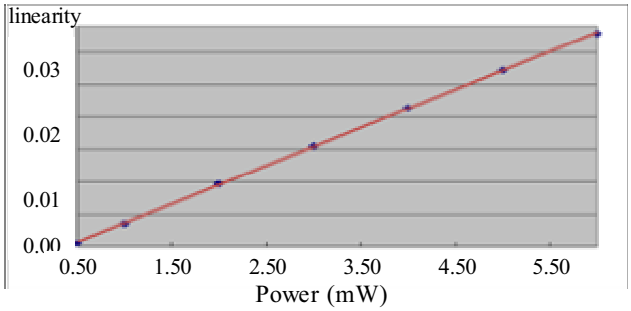

Figure 9. Fitted curve of the thermopile linearity.

soldered on the board to create a copper-nickel thermocouple. Fig. 8 shows the thermopile, which has 28 copper-nickel thermocouples, 202.5 Ω resistance, and 6.5 μV/mW sensitivity.

To measure the linearity of the thermopile, seven dc power levels from 0.5 mW to 6 mW are selected. Based on the results shown in Fig. 9, the linearity of this thermopile is 0.9999.

2.6. Measurement Process of the Calorimeter

The measurement process of the calorimeter is as follows. First, the temperature of the outer bucket is stabilized, and then the unknown rf power is input. After the temperature has been stabilized, the signal source is turned down, and the temperature decreases; the thermopile output e_1 at stable temperature is recorded. Next, dc power is fed into the calorimeter, and after the temperature has been stabilized, the thermopile output e_2 is recorded. The dc source is then turned down, and the thermopile stability output e_3 is recorded. Finally, rf power is input, and the thermopile stability output e_4 is recorded. The dc substitution power $P_{\mathrm{dc,\,sub}}$ can be calculated as:

$$\frac{P_{\mathrm{dc,\,sub}}}{P_{\mathrm{dc}}} = \frac{e_{\mathrm{rf}}}{e_{\mathrm{dc}}} = \frac{e_4 - e_3}{e_2 - e_1} \tag{4}$$

where $P_{\mathrm{dc}} = V^2/R$ is the dc power, V the dc voltage of the dc heater, R the operating resistance of the dc heater, and e_{dc} and e_{rf} are thermopile output voltages with dc and rf power inputs, respectively. This method can reduce the initial temperature drift effect of the input power. Fig. 10 shows the measurement process, and Fig. 11 presents the measurement system.

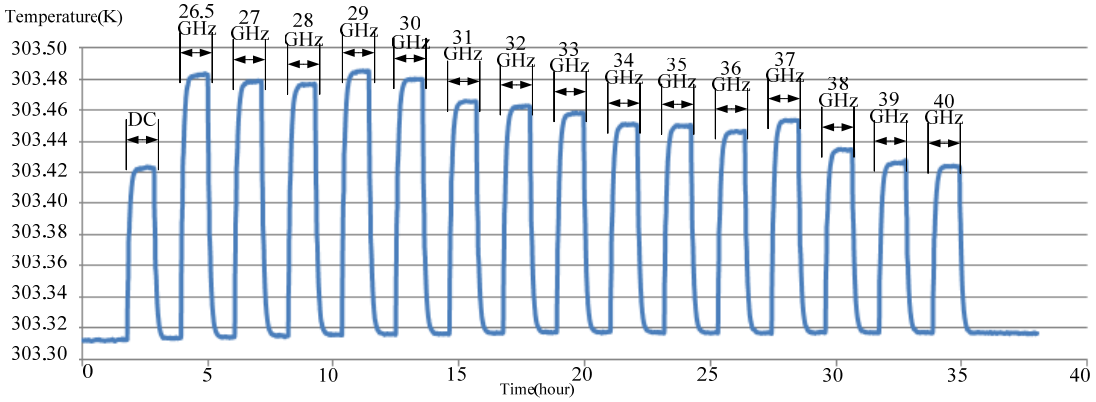

Figure 10. Measurement process of the calorimeter.

Figure 11. Measurement system of the calorimeter.

3. EFFECTIVE EFFICIENCY EVALUATION AND UNCERTAINTY ANALYSES

3.1. Effective Efficiency Evaluation

According to its definition, the effective efficiency of a calorimeter can be determined by the calorimetric measurement of the substituted dc power $P_{\mathrm{dc,\,sub}}$ on the load with respect to the total absorbed rf power P_{rf} on the calorimeter. According to Eq. (4), effective efficiency of calorimeter η can be calculated as:

$$\eta = \frac{P_{\mathrm{dc,\,sub}}}{P_{\mathrm{rf}}} \tag{5}$$

Equation (5) can be transferred to:

$$\eta = \frac{P_{\mathrm{dc,\,sub}}}{P_{\mathrm{rf}}} = \frac{P_{\mathrm{dc,\,sub}}}{P_L}\frac{P_L}{P_{\mathrm{rf}}} = \eta_{se}\eta_{te} \tag{6}$$

where P_L is the rf power absorbed by the load, and η_{te} is the transfer efficiency of the calorimeter, which can be defined by Eq. (7).

$$\eta_{te} = \frac{P_L}{P_{\mathrm{rf}}} = \frac{|S_{21}|^2\left(1-|\Gamma_L|^2\right)}{|1-S_{22}\Gamma_L|^2 - |(S_{12}S_{21}-S_{11}S_{22})\Gamma_L + S_{11}|^2} \tag{7}$$

The S parameters are those of the thermal isolation line; Γ_L is the reflection coefficient of the load. A vector network analyzer is used to measure S_{11}, S_{12}, S_{21}, and S_{22} of the isolation line, and Γ_L of the load.

η_{se} is the substitution efficiency of the calorimeter, which can be defined by Eq. (8).

$$\eta_{se} = \frac{P_{\mathrm{dc,\,sub}}}{P_L} \tag{8}$$

With dc power input, the thermopile output voltage e_{dc} is:

$$e_{\mathrm{dc}} = kP_{dc} = \frac{kV^2}{R_0}. \tag{9}$$

k is the thermal transfer constant between the load and the thermopile.

With rf power input, the thermopile output voltage e_{rf} is:

$$e_{\mathrm{rf}} = k(P_b + aP_w + bP_i). \tag{10}$$

P_b is the power absorbed by the absorber of the load and the power loss on the waveguide of the load, P_w the power loss on the flange of the load, P_i the power loss on the thermal isolation line, and a and b are constants of the thermal transfer path. Because a thermopile is installed on the waveguide of the load, the thermal transfer path constant of P_b is 1. P_L is the power absorbed by the load, and $P_b + P_w = P_L$.

Equation (10) can be transferred to

$$e_{\mathrm{rf}} = kP_L\left(\frac{P_b}{P_L} + \frac{aP_w}{P_L} + \frac{bP_i}{P_L}\right) \tag{11}$$

Combining Eqs. (4), (8), (9), (10), and (11) gives the substitution efficiency η_{se} at each frequency:

$$\eta_{se} = \frac{P_b}{P_L} + \frac{aP_w}{P_L} + \frac{bP_i}{P_L} \tag{12}$$

where a and b can be confirmed by a separate measurement with a low thermal capacity thin-metal short circuit on the input port of the load (for measuring a) and between the flange and waveguide of the load (for measuring b). P_b can be verified based on the dc substitution power, whereas P_w/P_L can be confirmed by measuring the scattering parameters of a same size flange with the flange of the load.

The isolation line of the calorimeter has a good thermal isolation effect, similar to that of air; thus, b is nearly equal to zero. The flange of the load is 2 mm long, compared with the waveguide of the load, which is 85 mm long; thus, the power loss on the flange can be ignored, and a is nearly equal to zero. Hence, η_{se} is nearly equal to 1, and $\eta = \eta_{te}$. Table 2 shows the effective efficiency measurement results.

Table 2. Effective efficiency measurement results.

Frequency (GHz)	26.5	27	28	29	30	31	32	33
Effective efficiency	0.9177	0.9259	0.9191	0.9247	0.9306	0.9144	0.9236	0.9378
Frequency (GHz)	34	35	36	37	38	39	40	−−
Effective efficiency	0.9331	0.9224	0.9252	0.9342	0.9307	0.9140	0.9213	−−

3.2. Uncertainty Analyses

The uncertainty of the calorimeter comes mainly from the following:

1) Substitution error

Based on the substitution efficiency experiment, the substitution error is almost $0.1\% \sim 0.5\%$. The uncertainty follows a uniform distribution, with a coverage factor of $\sqrt{3}$. The standard uncertainty is $0.06\% \sim 0.29\%$.

2) Transmission efficiency measurement error

Based on the transmission efficiency measurement, the efficiency error is $0.1\% \sim 0.5\%$. The uncertainty has a uniform distribution, with a coverage factor of $\sqrt{3}$. The standard uncertainty is $0.06\% \sim 0.29\%$.

3) dc power error

A digital voltmeter and the standard resistance are used to measure the dc power. The uncertainty comes from voltage error, resistance error, and lead resistance error. All the uncertainties follow a uniform distribution, with a coverage factor of $\sqrt{3}$. The standard uncertainty is 0.008%.

4) Temperature stability error

The temperature stability is 0.1%. The uncertainty has a uniform distribution, with a coverage factor of $\sqrt{3}$. The standard uncertainty is 0.06%.

5) Signal source amplitude stability error

During the measurement, a power sensor with high linearity is used to monitor the output power of the signal source. The amplitude stability error is less than 0.5%, and the uncertainty follows a uniform distribution, with a coverage factor of $\sqrt{3}$. The standard uncertainty is 0.29%.

6) Thermopile measurement error

The temperature difference of the calorimeter is measured by using a thermopile with an accuracy higher than 0.1%. The uncertainty has a uniform distribution, with a coverage factor of $\sqrt{3}$. The standard uncertainty is 0.06%.

7) Connector repeatability error

The uncertainty caused by connector repeatability is evaluated as type A. Six measurement results are used, with a standard deviation of less than 0.2%. The uncertainty is 0.2%.

Table 3 shows the uncertainty of the effective efficiency.

Table 3. Uncertainty of the calorimeter.

Source	Description	Type	Distribution	Coverage factor	Uncertainty
u_1	Substitution error	B	Uniform	$3^{1/2}$	$0.06\% \sim 0.29\%$
u_2	Effective efficiency error	B	Uniform	$3^{1/2}$	0.06%˜0.29%
u_3	dc power	B	Uniform	$3^{1/2}$	0.008%
u_4	Temperature stability	B	Uniform	$3^{1/2}$	0.06%
u_5	Source stability	B	Uniform	$3^{1/2}$	0.29%
u_6	Temperature accuracy	B	Uniform	$3^{1/2}$	0.06%
u_7	Repeatability	A			0.2%
u_c	Combined standard uncertainty				$0.37\% \sim 0.55\%$
U	Expanded uncertainty			2	$0.74\% \sim 1.1\%$

In the case that the coverage factor is 2, the confidence probability is 95.45%, and the expanded uncertainty of effective efficiency is $0.74\% \sim 1.1\%$.

4. EFFECTIVE EFFICIENCY VERIFICATION

4.1. Effective Efficiency Verification Experiment

After the evaluation of the effective efficiency of the calorimeter, the power sensor was calibrated through direct comparison method [5] by our calorimeter (WR-28), and then sent to the National Physical Laboratory (NPL) in the United Kingdom for calibration.

Because the transfer power standard in NPL has the same accuracy level as our calorimeter, the two uncertainties (our calorimeter and the NPL's transfer standard) do not meet the relationship twice. If the calibration results for the power sensor and the uncertainty satisfy Eq. (13), then our uncertainty of calorimeter can be proved reliable.

$$\frac{|K_a - K_b|}{K_a} \leq \sqrt{\left(U_a^2 + U_b^2\right)} \tag{13}$$

K_a is the calibration factor of the power sensor calibrated by our calorimeter, K_b the calibration factor of the power sensor calibrated by NPL, U_a the expanded uncertainty of our calorimeter, and U_b the expanded uncertainty of transfer power standard in NPL.

4.2. Verification Results

Three frequency points (26.5 GHz, 33 GHz, and 40 GHz) were selected to verify the effective efficiency of our calorimeter. The results are shown in Table 4.

Table 4. Verification results.

Frequency (GHz)	K_a (calorimeter)	K_b (NPL)	$\lvert K_a - K_b\rvert / K_a(\%)$	$\sqrt{U_a^2 + U_b^2}(\%)$
26.5	0.948	0.939	0.949	1.25
33	0.948	0.941	0.738	1.75
40	0.921	0.924	0.326	1.86

As shown in Table 4, $|K_a - K_b|/K_a$ is less than 1%, and the root mean square of the expanded uncertainty of the two standards is $1.25\% \sim 1.86\%$. Thus, Eq. (13) is satisfied, and the effective efficiency evaluation data and uncertainty analyses results can be considered as reliable.

5. CONCLUSION

The WR-28 dual-load waveguide calorimeter designed and manufactured in this study has high temperature stability, sensitivity, and accuracy. In future works, we plan to develop more realistic and accurate waveguide calorimeters of 170 GHz.

REFERENCES

1. Fantom, A., *Radiofrequency & Microwave Power Measurement*, Peter Peregrinus Ltds., England, 1990.
2. Sucher, M. and H. J. Carlin, "Broadband calorimeters for the measurement of low and medium level microwave power, I: Analysis and design," *IRE Trans.*, Vol. 6, No. 2, 189–194, Apr. 1958.
3. James, A. V. and L. O. Sweet, "Broadband calorimeters for the measurement of low and medium level microwave power, II: Construction and performance," *IRE Trans.*, Vol. 6, No. 2, 195–202, Apr. 1958.
4. Feng, X. and Y. Wu, "A broadband coaxial low power standard," *Acta Metrologica Sinica*, Vol. 1, 299–302, Oct. 1980.
5. Juroshek, J. R., "NIST 0.05 $\sim$ 50 GHz direct comparison power calibration system," *Conference on Presicion Electromagnetic Measurements Digest*, Vol. 30, No. 1, 166–167, 2000.